

# A High Order Numerical Scheme for Incompressible Navier-Stokes Equations

Hassan Khurshid<sup>1C</sup> and Klaus A. Hoffmann<sup>2</sup>

<sup>1</sup> Department of Mechanical Engineering, King Faisal University, K.S.A

<sup>2</sup> Department of Aerospace Engineering, Wichita State University, U.S.A

Received: 16/11/2013 – Revised 14/05/2014 – Accepted 03/06/2014

## Abstract

To solve the incompressible Navier-Stokes equations in a generalized coordinate system, a high order solver is presented. An exact projection method/fractional-step scheme is used in this study. Convective terms of the Navier-Stokes (N-S) equations are solved using fifth-order WENO spatial operators, and for the diffusion terms, a sixth-order compact central difference scheme is employed. The third-order Runge-Kutta (R-K) explicit time-integrating scheme with total variation diminishing (TVD) is adopted for the unsteady flow computations. The advantage of using a WENO scheme is that it can resolve applications using less number of grid points. Benchmark cases such as, driven cavity flow, Taylor-Green (TG) vortex, double shear layer, backward-facing step, and skewed cavity are used to investigate the accuracy of the scheme in detail for two dimensional flow. The code is further extended to three dimensions thus increasing the utility of the developed code for more complex problems. A simple example of flow through infinite long pipe has been solved in order to validate the 3D code.

*Keywords: WENO; incompressible flow; generalized coordinates; finite difference; shear layer problem.*

## 1. Introduction

The restriction to the incompressible flow introduces the computational difficulty that the continuity equation contains only velocity components and there is no obvious link with the pressure as there is for compressible equations. To overcome this restriction various numerical schemes are available to obtain the numerical solution of incompressible Navier-Stokes (N-S) equations. These include the marker and cell (MAC) method, spectral methods, semi-implicit method for pressure linked equations (SIMPLE), methods that use stream functions and vorticity variables, and exact projection methods. The exact projection method was originally proposed by Chorin [1] for incompressible, unsteady (N-S) equations, and subsequently it was further investigated by Drikakis and Rider [2]. This method is stable and can be used in applications with difficult boundary conditions. Therefore, in the current effort, a form of projection method, referred to as the fractional-step scheme, by Moin and Kim [3], is adopted with the collocated grid.

<sup>C</sup> Corresponding Author: Hassan Khurshid

Email: [hassankimr@gmail.com](mailto:hassankimr@gmail.com)

© 2014 All rights reserved. ISSR Journals

Traditional linearly stable schemes, such as spectral methods [4,5] and high-order spatial central difference methods [6,7] are suitable for cases where the solution can be fully resolved, but typically produces signs of instability when small-scale features of the flow, such as shears and roll-ups, cannot be adequately resolved on the computational grid. Although, in principle, one can always overcome this difficulty by refining the grid, today's computer capacity seriously restricts the largest possible domain size. For high Reynolds number flows or flows with strong shear, these schemes do not provide accurate results. As is well known, the high resolution shock capturing schemes, such as essentially non-oscillatory (ENO) and weighted essentially non-oscillatory (WENO) schemes, are based on the philosophy of giving up fully resolving rapid transition regions or shocks, just to capture them in a stable and somehow globally correct fashion, but, at the same time, requiring a high resolution for the smooth part of the solution. The success of such an approach for conservation laws is documented by several researchers [8, 9]. The conclusion seems to be that, when fully resolving a flow that is either impossible or too costly, a capturing scheme such as ENO can be used on a coarse grid to obtain at least some partial information about it. Thus, it is expected that, for the incompressible flow, one can use high-order ENO or WENO schemes on a coarse grid, without fully resolving the flow, but obtaining useful information.

Pioneering work in applying shock capturing compressible flow techniques to incompressible flows was performed by Bell et al. [10], who considered a second-order Godunov type discretization, investigated the projection into divergence-free velocity fields for general boundary conditions, and discussed the accuracy of time discretizations. Higher-order ENO and WENO schemes for incompressible flows are extensions of such methods.

ENO schemes were introduced by Harten et al. [11] in the form of cell averages. Their procedure used an adaptive stencil of grid points, and consequently, the resulting schemes were highly non-linear. Since the publication of that original paper, the authors and many other researchers have followed this pioneering work, improving the methodology and expanding the range of its applications [12-17]. ENO schemes are high order accurate; however, they have some drawbacks, as outlined by Jiang and Shu [18]. The ENO scheme was modified to the WENO scheme by Jiang and Shu [18] and by Liu et al. [13]. In the WENO scheme, instead of using only one candidate stencil, a convex combination of all candidate stencils is used. Each of the candidate stencils is assigned a weight, which determines the contribution of this stencil to the final approximation of the numerical flux. Weights are defined in such a way that, in smooth regions, they approach certain optimal weights to achieve a high order of accuracy, while in the region near discontinuities; stencils that contain the discontinuities are assigned a nearly zero weight. The WENO scheme has been further improved by Arshed and Hoffmann [19] who improved the accuracy of the WENO scheme near the critical points and also reduced the severe smearing at contact discontinuities.

The WENO scheme is a shock capturing scheme, however, more recently it has been used in solving incompressible flows as well. Chen et al. [20] used implicit WENO schemes to solve incompressible Navier-Stokes equations by selecting their algorithm on the artificial compressibility formulation. They presented a class of lower-upper/approximate factorization implicit WENO scheme. Symmetric Gauss-Seidel relaxation was used to compute steady state solutions, while symmetric successive over relaxation was used to treat time dependent flows. Hsieh et al. [21] investigated several variants of WENO schemes numerically for Euler equations

In the current effort, the WENO scheme of Shu [22] is adopted and applied to solve incompressible flow problems. *Flux splitting is used, and the WENO scheme is applied to the convective terms without introducing artificial compressibility. This is the main difference in the method as compared to [20] that makes the implementation simpler. In addition the resulting scheme has been tested not only on the simple rectangular geometries but also on complex geometries such as skewed cavity where coordinate transformation is required and the code has been extended in order to solve three dimensional problems as well.* A sixth-order compact scheme is applied to solve the viscous terms. The fractional-step scheme in conjunction with third-order

Runge Kutta (R-K) total variation diminishing (TVD) is used for the time discretization. The R-K TVD is generally good, since it preserves the variation. A Poisson solver based on compact scheme is used in order to find the pressure and consequently the velocity at the new time level is calculated by applying the pressure correction. The resulting scheme is applied to standard incompressible flow problems.

## 2. Numerical procedure

Numerical procedure to solve two dimensional incompressible problems is the same as given in [23]. In order to extend the code from two dimensions to three dimensions following governing equations and procedure is followed.

### 2.1. 3D Pressure Projection and 3D System of Equations

The equations in Cartesian coordinate system can be written as

$$\frac{\partial Q}{\partial t} = \frac{\partial(E_v - E)}{\partial x} + \frac{\partial(F_v - F)}{\partial y} + \frac{\partial(G_v - G)}{\partial z} \tag{1}$$

with

$$Q = \begin{bmatrix} u \\ v \\ w \end{bmatrix} \quad E = \begin{bmatrix} u^2 \\ uv \\ uw \end{bmatrix} \quad F = \begin{bmatrix} uv \\ v^2 \\ vw \end{bmatrix} \quad G = \begin{bmatrix} uv \\ vw \\ w^2 \end{bmatrix} \tag{2}$$

$$E_v = \text{Re}^{-1} \begin{bmatrix} 2u_x \\ u_y + v_x \\ u_z + w_x \end{bmatrix} \quad F_v = \text{Re}^{-1} \begin{bmatrix} v_x + u_y \\ 2v_y \\ v_z + w_y \end{bmatrix} \quad G_v = \text{Re}^{-1} \begin{bmatrix} u_z + w_x \\ v_z + w_y \\ 2w_z \end{bmatrix}$$

where  $u, v,$  and  $w$  are velocities in the Cartesian coordinate system, and indexes represent derivation with respect to that index, for example  $v_x = dv/dx$ . Conventionally, equation (1) is transformed into the generalized coordinates  $(\xi, \eta, \zeta)$  as

$$\frac{\partial \hat{Q}}{\partial t} = \frac{\partial(\hat{E}_v - \hat{E})}{\partial \xi} + \frac{\partial(\hat{F}_v - \hat{F})}{\partial \eta} + \frac{\partial(\hat{G}_v - \hat{G})}{\partial \zeta} \tag{3}$$

where

$$\hat{Q} = J \begin{bmatrix} u \\ v \\ w \end{bmatrix} \quad \hat{E} = J \begin{bmatrix} uU \\ vU \\ wU \end{bmatrix} \quad \hat{F} = J \begin{bmatrix} uV \\ vV \\ wV \end{bmatrix} \quad \hat{G} = J \begin{bmatrix} uV \\ vV \\ wV \end{bmatrix}$$

$$\hat{E}_v = J \left[ \xi E_v + \eta F_v + \zeta G_v \right] \quad \hat{F}_v = J \left[ \xi E_v + \eta F_v + \zeta G_v \right] \quad \hat{G}_v = J \left[ \xi E_v + \eta F_v + \zeta G_v \right]$$

$$U = \xi u + \eta v + \zeta w, V = \xi u + \eta v + \zeta w, W = \xi u + \eta v + \zeta w, J = 1 / \left| \begin{matrix} x & x & x \\ y & y & y \\ z & z & z \end{matrix} \right|$$

Poisson equation uses the derivative operator to solve the Poisson equation; therefore, the left hand side shows an operator of the second derivative  $\nabla$  acting on pressure  $P$ , and on the right side, the term is constructed according to the coordinate system transformation as

$$\Upsilon P = \frac{1}{J\Delta t} \left( \frac{\partial(JU)}{\partial} + \frac{\partial(JV)}{\partial} + \frac{\partial(JW)}{\partial} \right) \quad (5)$$

where  $U, V$ , and  $W$  have the same definition as above. The derivative operator is

$$\Upsilon = \frac{\partial}{\partial q_j} \left( \frac{\partial}{\partial q_k} \frac{\partial q_k}{\partial x_i} \right) \frac{\partial q_j}{\partial x_i} \quad (6)$$

where  $i, j, k = \{1, 2, 3\}$ ,  $q_1 = u$ ,  $q_2 = v$ , and  $q_3 = w$ .

For the three-dimensional case, velocity correction equation is modified as

$$\begin{aligned} (u)^{n+1} &= (u)^* - (P_x + P_y + P_z) \Delta t \\ (v)^{n+1} &= (v)^* - (P_x + P_y + P_z) \Delta t \\ (w)^{n+1} &= (w)^* - (P_x + P_y + P_z) \Delta t \end{aligned} \quad (7)$$

## 2.2. 3D Pressure Projection and 3D System of Equations

The main idea here is the same as applied in the numerical procedure of 2D [23]—that is to employ WENO for the convective part and a compact method to solve the viscous portion of Navier-Stokes equation.

## 2.3. Convective Part

In three dimensions, there are three fluxes:  $\hat{E}, \hat{F}, \hat{G}$ . The flux derivative and flux splitting are performed using the same method as described [23]. However, the  $\Lambda$  matrix for flux splitting and vectors of the characteristic flow field are different now. The  $\Lambda$  matrix for the  $\hat{E}$  flux is

$$\begin{bmatrix} |x^u + y^v + z^w| & 0 & 0 \\ 0 & 2|x^u + y^v + z^w| & 0 \\ 0 & 0 & |x^u + y^v + z^w| \end{bmatrix} \quad (8)$$

for flux  $\hat{F}$  is

$$\begin{bmatrix} |x^u + y^v + z^w| & 0 & 0 \\ 0 & 2|x^u + y^v + z^w| & 0 \\ 0 & 0 & |x^u + y^v + z^w| \end{bmatrix} \quad (9)$$

and for  $\hat{G}$  is

$$\begin{bmatrix} |x^u + y^v + z^w| & 0 & 0 \\ 0 & 2|x^u + y^v + z^w| & 0 \\ 0 & 0 & |x^u + y^v + z^w| \end{bmatrix} \quad (10)$$

The right/left eigenvalues for  $\hat{E}$  are

$$r = \begin{bmatrix} -\bar{y} & \bar{u} & -\bar{z} \\ -\bar{x} & \bar{v} & 0 \\ 0 & \bar{w} & -\bar{x} \end{bmatrix}, l = \frac{1}{\bar{u}\bar{x} + \bar{v}\bar{y} + \bar{w}\bar{z}} \begin{bmatrix} -\bar{v} & \bar{u} + \bar{w}\bar{z}/\bar{x} & -\bar{v}\bar{z}/\bar{x} \\ -\bar{x} & \bar{w}\bar{y}/\bar{x} & \bar{z} \\ -\bar{w} & \bar{w}\bar{y}/\bar{x} & -\bar{u} - \bar{v}\bar{y}/\bar{x} \end{bmatrix} \quad (11)$$

for  $\hat{F}$  are

$$r = \begin{bmatrix} -\bar{y} & \bar{u} & 0 \\ -\bar{x} & \bar{v} & -\bar{z} \\ 0 & \bar{w} & -\bar{y} \end{bmatrix}, l = \frac{1}{\bar{u}\bar{x} + \bar{v}\bar{y} + \bar{w}\bar{z}} \begin{bmatrix} -\bar{v} - \bar{w}\bar{z}/\bar{y} & \bar{u}_x & -\bar{w}\bar{z}/\bar{y} \\ -\bar{x} & \bar{y} & \bar{z} \\ \bar{w}\bar{x}/\bar{y} & \bar{w} & -\bar{v} - \bar{u}_x/\bar{y} \end{bmatrix} \quad (12)$$

and for  $\hat{G}$  are

$$r = \begin{bmatrix} -\bar{z} & \bar{u} & 0 \\ 0 & \bar{v} & -\bar{z} \\ -\bar{x} & \bar{w} & -\bar{y} \end{bmatrix}, l = \frac{1}{\bar{u}\bar{x} + \bar{v}\bar{y} + \bar{w}\bar{z}} \begin{bmatrix} \bar{w} + \bar{v}\bar{y}/\bar{z} & -\bar{x} & -\bar{v}\bar{z}/\bar{z} \\ -\bar{u}\bar{y}/\bar{z} & -\bar{y} & \bar{w} + \bar{u}_x/\bar{z} \\ -\bar{u} & \bar{z} & -\bar{v} \end{bmatrix} \quad (13)$$

**2.4. Viscous Part**

The 3D code requires three separate compact differential operators  $D$  in the three directions:  $(D^x)$ ,  $(D^y)$ , and  $(D^z)$ . In order to differentiate, the nested differentiation rule is applied; for example,  $u_x$  is

$$u_x = (D^z u)_x + (D^y u)_{y_x} + (D^x u)_{x_x} \quad (14)$$

**2.5. Poisson Solver**

A few modifications to cover the third direction are made in the basic 2D code. For the right side  $S$ , the formula used is

$$S_{ijk} = \frac{1}{J_{ijk} \Delta t} (\sum_m D_{im}^x (JU)_{mjk} + \sum_m (JV)_{imk} D_{mj}^y + \sum_m (JW)_{ijm} D_{mk}^z) \quad (15)$$

The pressure is calculated by means of iterative solver where its next estimation is covered by the following equation:

$$\begin{aligned}
 P_{ijk}^{n+1} = & \frac{S_{ijk} - \sum_{l>i} \ell_{il}^{xx} P_{ljk}^n - \sum_{l<i} \ell_{il}^{xx} P_{ljk}^{n+1}}{\ell_{ii}^{xx} + \ell_{jj}^{yy} + \ell_{kk}^{zz}} \\
 & + \frac{-\sum_{m>j} P_{imk}^n \ell_{mj}^{yy} \sum_{m<j} P_{imk}^{n+1} \ell_{mj}^{yy}}{\ell_{ii}^{xx} + \ell_{jj}^{yy} + \ell_{kk}^{zz}} \\
 & + \frac{-\sum_{q>k} P_{ijq}^n \ell_{qk}^{zz} \sum_{q<k} P_{ijq}^{n+1} \ell_{qk}^{zz}}{\ell_{ii}^{xx} + \ell_{jj}^{yy} + \ell_{kk}^{zz}}
 \end{aligned} \tag{16}$$

where

$$\begin{aligned}
 \ell_{ij}^{xx} &= \sum_m (D^x \langle_x)_{im} (D^x \langle_x)_{mj} + \sum_m (D^x \langle_y)_{im} (D^x \langle_y)_{mj} + \sum_m (D^x \langle_z)_{im} (D^x \langle_z)_{mj} \\
 \ell_{ij}^{yy} &= \sum_m (D^y \langle_x)_{im} (D^y \langle_x)_{mj} + \sum_m (D^y \langle_y)_{im} (D^y \langle_y)_{mj} + \sum_m (D^y \langle_z)_{im} (D^y \langle_z)_{mj} \\
 \ell_{ij}^{zz} &= \sum_m (D^z \langle_x)_{im} (D^z \langle_x)_{mj} + \sum_m (D^z \langle_y)_{im} (D^z \langle_y)_{mj} + \sum_m (D^z \langle_z)_{im} (D^z \langle_z)_{mj}
 \end{aligned} \tag{17}$$

Finally, the pressure correction terms are

$$\begin{aligned}
 (u)^{n+1} &= (u)^* - (D^x p \langle_x + p D^y \langle_y + p D^z \langle_z) \Delta t \\
 (v)^{n+1} &= (v)^* - (D^x p \langle_y + p D^y \langle_y + p D^z \langle_z) \Delta t \\
 (w)^{n+1} &= (w)^* - (D^x p \langle_z + p D^y \langle_z + p D^z \langle_z) \Delta t
 \end{aligned} \tag{18}$$

### 3. Numerical Results and Discussion

The developed computer code is investigated using standard incompressible flow problems (two and three dimensional): driven cavity flow, Taylor-Green (TG) vortex problem, double shear layer, backward-facing step, skewed cavity problem and flow through infinite long pipe.

#### 3.1. Driven Cavity Flow

The driven cavity flow problem is a benchmark problem used to validate the incompressible flow solver. It is extensively investigated because of certain flow features. Some interesting features of this problem are the following: boundary layer on the wall, flow separation from one wall and reattachment on the perpendicular wall, attachment and separation from the same wall, multiple separation and attachment, vortices, and bubbles. Table 1 shows the value of the vorticity and the location of the primary vortex center obtained by different researchers using different numerical methods. The difference in the results of the present study as compared to the highly accurate spectral solutions of Botella and Peyret [24], extrapolated solutions of Schreiber and Keller [25] and fourth order solutions of Erturk and Gokcol [26], is very small. The current solutions are also comparing good with the other results of Wright and Gaskell [27], Benjamin and Denny [28], Nishida and Satofuka [29], Erturk, Corke and Gokcol [30] and Li, Tang and Fornberg [31] as shown in the table. The reason of reporting this table is to show that the results are obtained using very coarse grid and our proposition that WENO scheme resolves the flow with fewer grid points holds. The least amount of data points in the above table are 129 x 129 used by Li et al. [31] whereas the grid points used in current study are 80 x 80. All other numerical methods mentioned are using more grid points to achieve the said results. The similar location of the primary vortex center and close vorticity value indicates that the WENO scheme use is beneficial in getting the solution by using fewer grid points thus in the end

saving the computational time of the computer and giving useful information about the flow characteristics.

TABLE 1: VORTICITY VALUE AND LOCATION OF THE CENTER OF PRIMARY VORTEX BY DIFFERENT STUDIES

Reference	Grid size	Accuracy	Vorticity	x	y
Botella & Peyret	N=160	N=160	2.067753	0.5308	0.5652
Schreiber & Keller	Extrapolated	6 <sup>th</sup> order	2.0677		
Ertruk & Gokcol	601 <sup>2</sup>	4 <sup>th</sup> order	2.067760	0.5300	0.5650
Wright & Gaskell	1024 <sup>2</sup>	2 <sup>nd</sup> order	2.06997	0.5308	0.5659
Benjamin & Denny	Extrapolated	High order	2.078		
Nishida & Satofuka	129 <sup>2</sup>	8 <sup>th</sup> order	2.068546	0.5313	0.5625
Erturk et al.	513 <sup>2</sup>	2 <sup>nd</sup> order	2.064765	0.5313	0.5645
Li et al.	129 <sup>2</sup>	4 <sup>th</sup> order	2.05876	0.5313	0.5625
Current Study	80 <sup>2</sup>	5 <sup>th</sup> order	2.06893	0.5316	0.5642

### 3.2. Taylor Green Vortex Problem

The Taylor-Green vortex test problem has been widely used for verification of incompressible viscous flow solvers. The order of accuracy of the proposed solver is established by comparing the numerical results with the analytical values. A two-dimensional exact solution to the unsteady problem is provided by

$$\begin{aligned}
 u(x, y, t) &= -\cos(kx) \sin(ky) \exp(-2k^2t / \text{Re}) \\
 v(x, y, t) &= \sin(kx) \cos(ky) \exp(-2k^2t / \text{Re}) \\
 p(x, y, t) &= -\frac{1}{4}(\cos(kx) + \cos(ky)) \exp(-4k^2t / \text{Re})
 \end{aligned}
 \tag{19}$$

The numerical domain of the numerical solutions is a square of side 2 with periodic boundary conditions in both x and y-directions. Uniform grid points of 32<sup>2</sup>, 64<sup>2</sup>, 128<sup>2</sup>, 256<sup>2</sup> and 512<sup>2</sup> are used in this convergence rate study. The order of accuracy of the proposed scheme is established by numerical simulation of the Taylor-Green vortex test at Re = 100, for 100 steps with a fixed time step of 0.001. The maximum error and the convergence rates are shown in (Table 2). It can be seen clearly that convergence rate of fifth order for the velocity variables is obtained as the grid is refined.

TABLE 2: MAXIMUM ERROR AND CONVERGENCE RATES FOR TG VORTEX TEST

Variable	32 <sup>2</sup>	Rate	64 <sup>2</sup>	Rate	128 <sup>2</sup>	Rate	256 <sup>2</sup>	Rate	512 <sup>2</sup>
u	8.09e -4	3.7	6.2e -5	4.58	2.85e -6	4.99	0.897e-7	4.99	.0281e-7
v	8.42e -4	3.52	7.3e -5	4.927	2.4e -6	5.01	0.745e-7	5.005	.0232e-7

### 3.3. Double Shear Layer Test

The shear layer problem is an important numerical test in order to observe whether the numerical procedure is working properly when the solution of the problem is not smooth. This is a flow with a strong shear/discontinuous initial condition. A periodic boundary condition is applied everywhere on the boundaries and the initial condition of the jet is:

$$\begin{aligned}
 u_0(x, y) &= \begin{cases} \tanh(0.25 - y) / \dots, & y \leq 0.5 \\ \tanh(y - 0.75) / \dots, & y > 0.5 \end{cases} \\
 v_0(x, y) &= u \sin(2\pi x)
 \end{aligned}
 \tag{20}$$

Due to the initial condition, two shear layers are formed, since the velocity gradient is high at those two particular regions. In this case, the grid size is 256 x 256. Figure 1

provides the vorticity contours at  $t = 0.4, 0.8, 1.2,$  and  $1.8$ . These results are compared with the pioneering work of Bell et al. [10]. The pattern obtained with the current approach is in good agreement with the result previously published for shear layer flow. No distortions or oscillations can be observed in the evolution of the flow over the specific time period, and no spurious vortices are seen.

In Figure 2, vorticity contours at  $t = 1.8$  are shown for different grid sizes. It can be observed that even at the coarser grid the shape, location and number of vortices are maintained thus indicating the usefulness of WENO in getting the overall result by using fewer grid points. Figure 3 shows the plot of kinetic energy versus time for the double shear layer at two grid sizes of  $128^2$  and  $256^2$ . As the mesh becomes finer the kinetic energy stays unchanged for a longer period of time as compared to coarser grid. On comparing the current result of  $256^2$  grid size kinetic energy plot with the (Figure 4) in paper of Bell et al. [10], it is seen that the kinetic energy is decreasing appreciably from the start of the solution whereas in the current solver, it is constant upto  $t \sim 1.1$ . This clearly indicates that the new scheme has less dissipation than the original scheme of Bell et al. [10]. It is obvious to conclude that at meshes greater than  $256^2$  size the kinetic energy will be invariant for even greater time than 1.1.

### **3.4. Backward Facing Step**

Another commonly utilized benchmark problem is the flow over a backward-facing step. The dimensions of the step height and the channel length upstream and downstream are taken to be as reported in the experimental study of Armaly, Durst, Pereira and Schoung [32] and the numerical study of Choi and Barakat [33]. The dimensions are sufficiently large so that the flow is fully developed when it reaches the step. The length of the channel downstream is such that the recirculation zone produced behind the step is independent of the rest of the channel length. For this problem, a multi-block meshing approach was utilized, and the Navier–Stokes solver was modified accordingly.

Data points are obtained by digitizing the experimental data and comparing them to the numerical results, for a Newtonian fluid in Armaly et al. [32]. Figure 4 shows the comparison of velocity profiles obtained numerically with the experimental profiles at five positions downstream of the step. Two conclusions can be made by considering the comparison figures. First, the shape of the velocity profile obtained by the computer code is similar to the experimental profiles obtained by Armaly et al. [32]. The profile is parabolic right at the step, which indicates the fully developed flow. In the region where there is a circulation zone, the shape of velocity profile changes, but it becomes parabolic again as the flow moves downstream of the step. Second, the values of numerical simulation compare well with the experimental values. Figure 5 illustrates the comparison between the  $L/S$  (non-dimensional length of the recirculation zone) at different Reynolds numbers. Where  $L$  is the length of the channel after the step and  $S$  is the step height. The numerical values again compare well to the experimental values. Figure 6 provides the streamlines over the backward-facing step for  $Re = 50, 100, 200$  and  $400$ . It is clear that as the  $Re$  increases, the recirculation length also increases. The flow pattern is consistent with the results published by Choi and Barakat [33] in their numerical study. It is worth mentioning that their computational domain consisted of 14,600 rectangular elements for the numerical simulations, whereas the current study is using only 9000 nodes to obtain the same results. The reason for this is that the WENO scheme has the inherent property of resolving flow even if a coarser grid size is used. Moreover, Choi et al. [33] investigation uses the CFD software Fluent, which usually uses a third order solver for the spatial derivatives of N-S equations and second order solver for time discretization, where the current effort is making use of fifth and sixth order schemes to solve spatial derivatives (convective/diffusion) and a

third order scheme for temporal discretization. The higher order schemes result in more accuracy due to less truncation error.

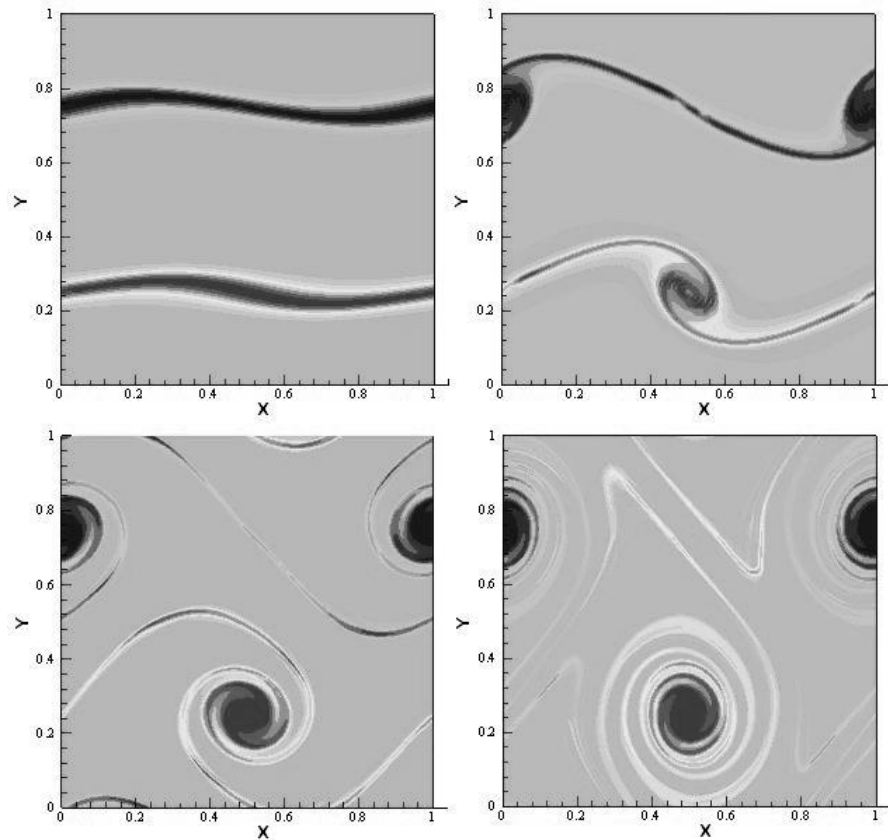


Figure 1. Vorticity contours for double shear layer flow at  $t = 0.4$  (top left),  $0.8$  (top-right),  $1.2$  (bottom-left), and  $1.8$  (bottom-right)

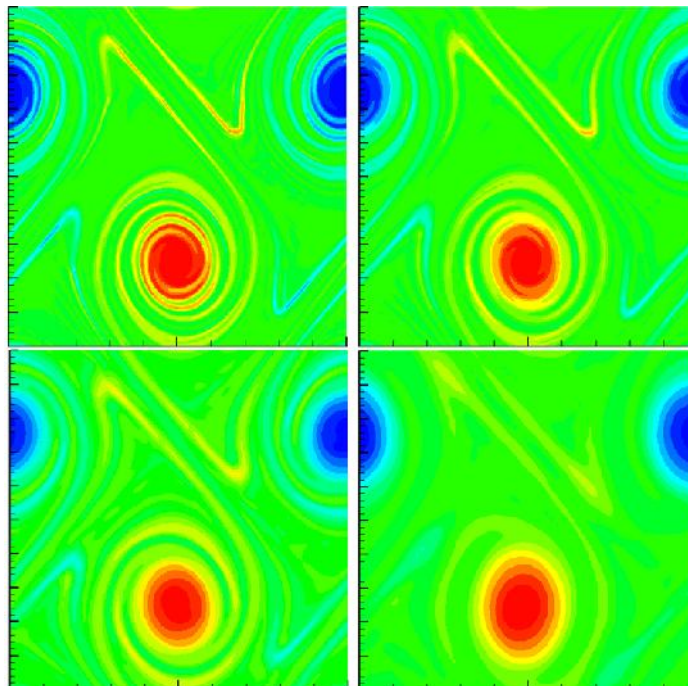


Figure 2. Vorticity contours for double shear layer flow at  $t = 1.8$  for grid sizes of  $256^2$  (top left),  $180^2$ (top-right),  $128^2$  (bottom-left) and  $64^2$ (bottom-right)

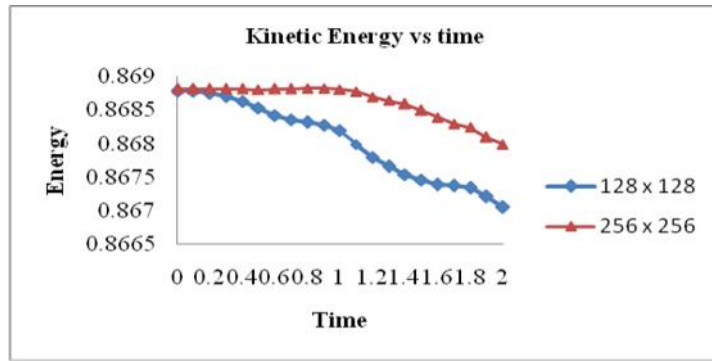


Figure 3. Kinetic energy versus time for double shear layer

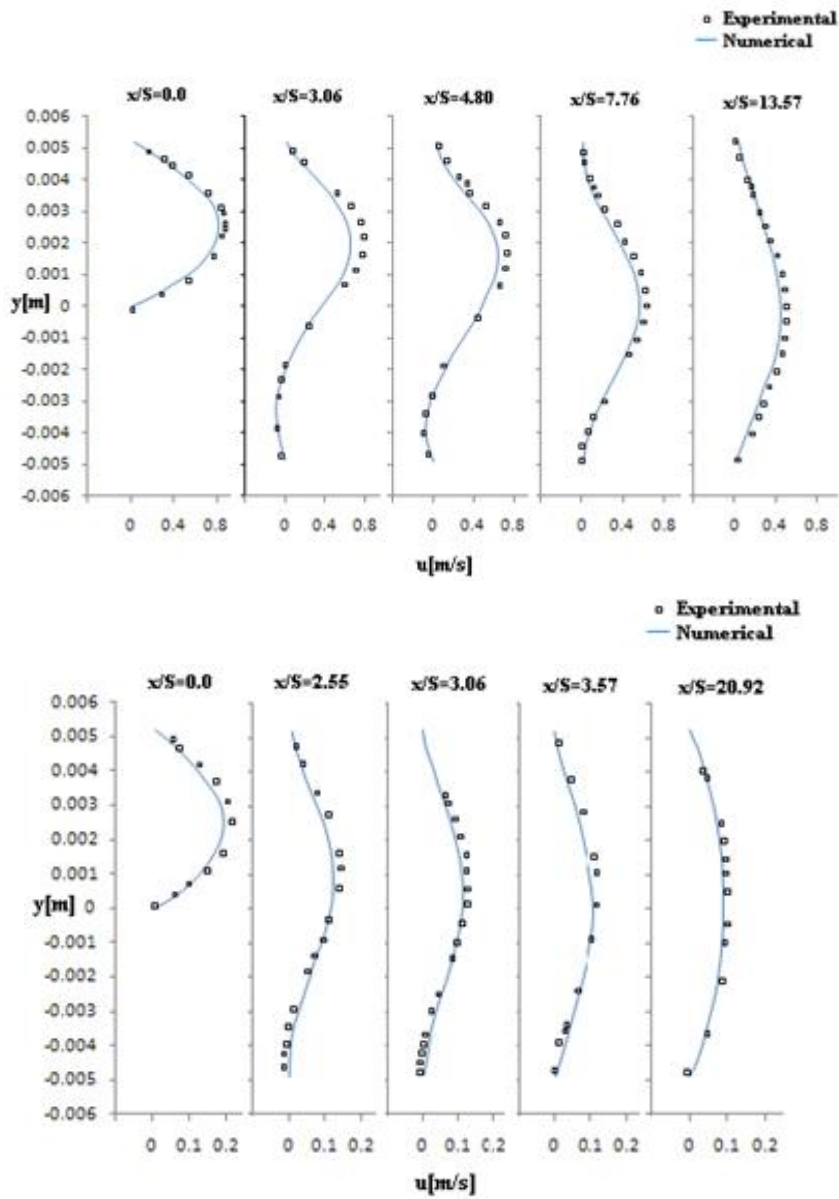


Figure 4. Axial velocity comparison for Newtonian steady flow at  $Re=100$  (top) and  $Re = 389$  (bottom)

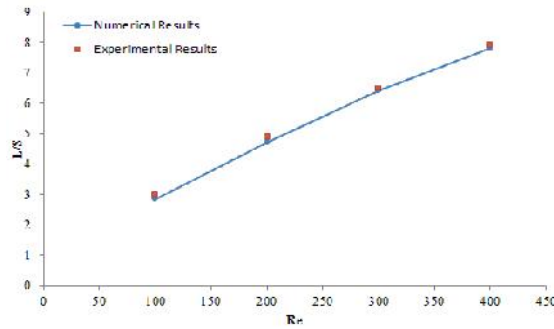


Figure 5. Non-dimensionalized length of recirculation region at different Re numbers

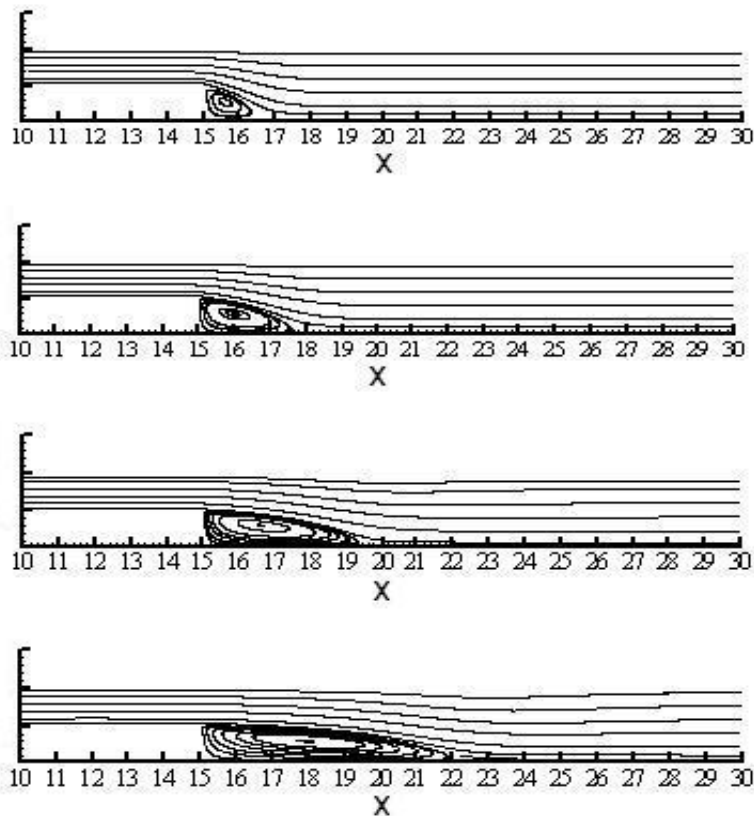


Figure 6. Streamlines of Newtonian flow at Re = 50,100,200, and 400

### 3.5. Skewed Cavity

Up to this point all the examples analyzed are of rectangular geometry. As the problems in real life mostly comprise of non-rectangular geometries so to test the developed solver for such kinds of problems is very essential. Benchmark problems with non-rectangular grids for numerical schemes to compare solution to each other are not many. Demirdzic, Lilek and Peric [34] presented the results for the skewed driven cavity for Re 100 and 1000 for the skewed angles of 45 and 30 degrees. Their results serve as a benchmark solution for the non-rectangular grid test. The solution was obtained by using the multigrid finite volume method with grids up to 320 x 320 control volumes. This problem is simple to implement, and one can easily verify whether the code is functioning properly or not by comparing the results with the skewed cavity results of Demirdzic et al. [34]. In the current study, a grid size of 128 x 128 (16,384 cells) is used, and the numerical results are in

close agreement to the results of Demirdzic et al. [34] that were obtained at 102,400 cells. Schematic of skewed driven cavity is drawn in Figure 7.

Figure 8 shows the  $u$ -velocity along the vertical line and  $v$ -velocity along the horizontal line passing through the geometric center of the skewed cavity for  $Re$  100 and 1000 at the skewed angle of 45 degrees. Figure 9 illustrates the  $u$ -velocity along the vertical line and  $v$ -velocity along the horizontal line passing through the geometric center for  $Re$  100 and 1000 at the skewed angle of 30 degrees. Other researchers that have performed the skewed driven cavity tests are Erturk and Dursun [35], Oosterlee, Wessling, Segal and Brakkee [36] and Shyklyar and Arbel [37] using the grid size of  $513^2$ ,  $256^2$  and  $320^2$  respectively as compared to our grid of  $128^2$ . This test clearly demonstrates that the proposed scheme is performing properly for the generalized coordinates in addition to the rectangular grid obtaining results at coarser grids when compared to the grid sizes of above mentioned researchers.

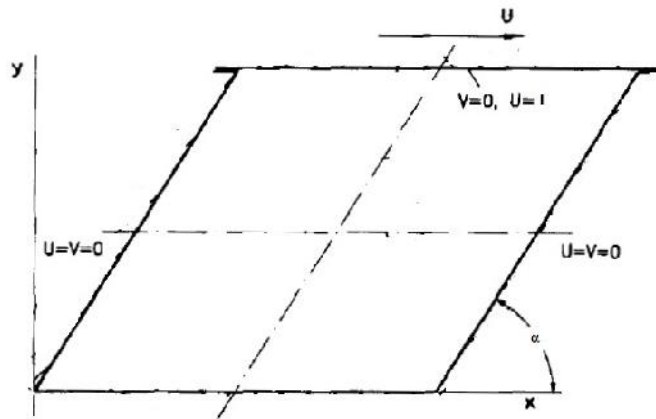


Figure 7. Geometric model of skewed driven cavity

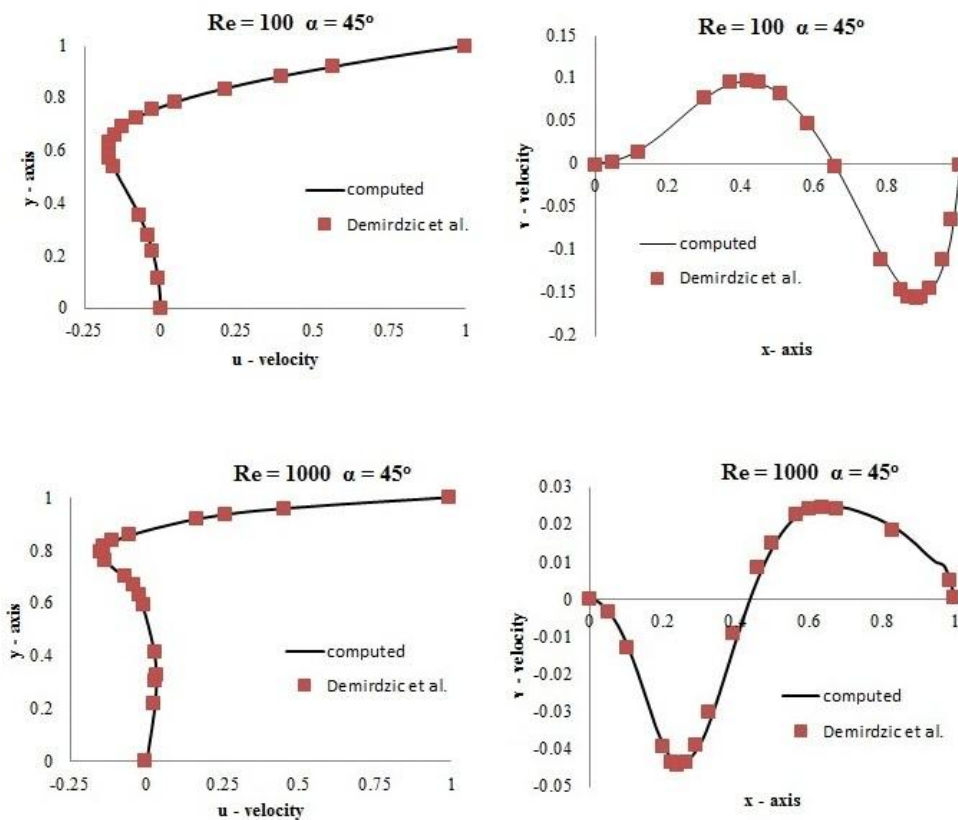


Figure 8.  $u$  and  $v$ -velocity profiles at  $Re = 100$  and  $1000$  for skewed angle of 45 degrees

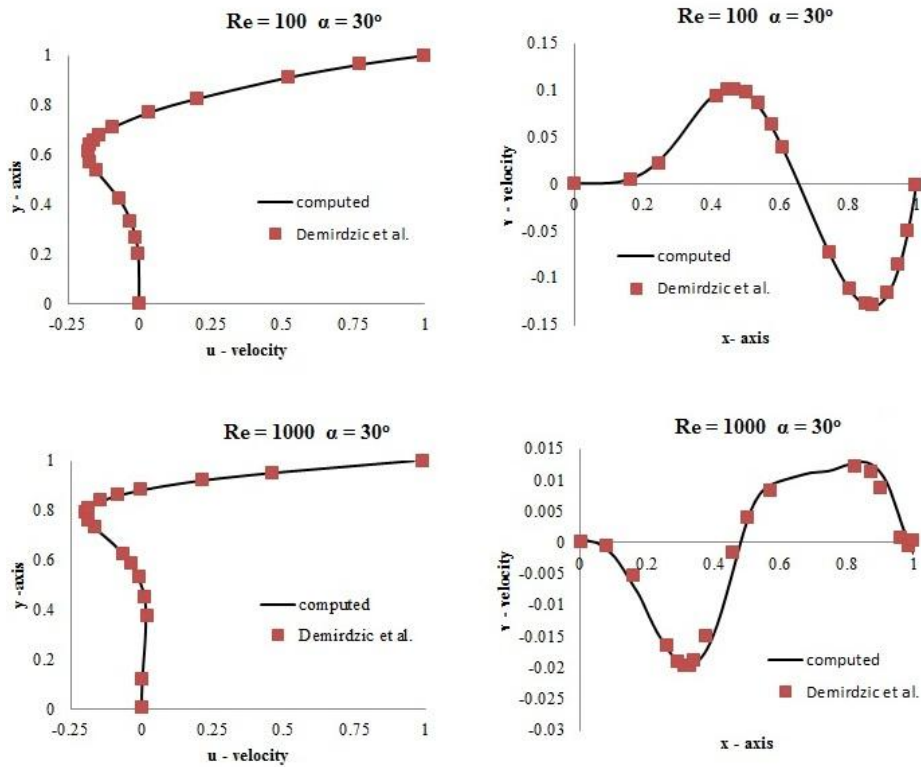


Figure 9. u and v-velocity profiles at Re = 100 and 1000 for skewed angle of 30 degrees

### 3.6. Flow through infinite long pipe

The 3D code is validated by comparing it with an analytical solution of a specific flow field. The analytical solution is derived from an incompressible Navier-Stokes equation as follows: The periodic boundary condition in  $x$  and  $z$  directions is applied for three-dimensional NS equations in the cylindrical coordinate system. This assumption makes all spatial derivatives in these directions zero, additional initial conditions are set as  $u_r = 0$  and  $u_\theta = 0$ , so the only non-zero velocity is  $u_z$ . As a result, the NS equation is reduced to a single differential equation of the form

$$\frac{\partial u_z}{\partial t} = \sim \left( \frac{\partial^2 u_z}{\partial r^2} + \frac{1}{r} \frac{\partial u_z}{\partial r} \right) \tag{21}$$

The solution of this equation can be proposed as

$$u_z(r, t) = \bar{u}(r) e^{-\tilde{S}t} \tag{22}$$

Substituting the proposition into equation (21) and rearranging yields

$$\frac{\partial^2 \bar{u}}{\partial r^2} + \frac{1}{r} \frac{\partial \bar{u}}{\partial r} + \frac{\tilde{S}}{\sim} \bar{u} = 0 \tag{23}$$

It can be further proposed that

$$\bar{u} = \sum_{n=0}^{\infty} a_n r^n \tag{24}$$

Introducing it into equation (23) results in

$$\sum_{n=2}^{\infty} n^2 a_n r^{n-2} + \frac{\tilde{S}}{\sim} \sum_{n=0}^{\infty} a_n r^n + \frac{a_1}{r} = 0 \tag{25}$$

In order to avoid singularity at the center ( $r = 0$ ),  $a_1$  is set to 0. Now, the summation can be skipped to find the relation for  $a_{n+2}$ :

$$a_{n+2} = -\frac{1}{n^2} \frac{\check{S}}{\sim} a_n \tag{26}$$

This enables us to calculate  $a_{n+2}$  from  $a_n$ . It is known that the variable  $a_1$  is equal to zero, thus making the value of every odd  $n$  equal to zero as well. However, from the initial conditions, it is also known that the flow at the center is ( $\bar{u}(0)=1$ ); hence,  $a_0=1$ . Therefore, the remaining  $a$ 's (for  $n$ =even) can be found as follows. For example,

$$\begin{aligned} a_0 &= 1 \\ a_2 &= -\frac{1}{4} \frac{\check{S}}{\sim} \\ a_4 &= \frac{1}{64} \left(\frac{\check{S}}{\sim}\right)^2 \\ a_6 &= -\frac{1}{2304} \left(\frac{\check{S}}{\sim}\right)^3 \\ a_8 &= \dots\dots\dots \end{aligned} \tag{27}$$

It is possible to prove that

$$\lim_{n \rightarrow \infty} a_n = 0 \tag{28}$$

and that this series is monotonic, which means that only  $n = 6$  elements of the series can be obtained to estimate the solution and keeping the error low. In fact, estimation with error lower than the round error of the floating number is required. The last unknown is  $S$ . However, it is known that velocity at the wall ( $r = R$ , but for simplicity let  $R = 1$ ) must be zero; therefore,  $\bar{u}(r=1) = 0$ . It follows that

$$1 - \frac{1}{4} \frac{\check{S}}{\sim} + \frac{1}{64} \left(\frac{\check{S}}{\sim}\right)^2 - \frac{1}{2304} \left(\frac{\check{S}}{\sim}\right)^3 = 0 \tag{29}$$

which provides  $\frac{\check{S}}{\sim} = 5.75$ . Finally, the analytical solution is

$$u_z(r,t) = \left[ 1 - \frac{1}{4} \frac{\check{S}}{\sim} r^2 + \frac{1}{64} \left(\frac{\check{S}}{\sim}\right)^2 r^4 - \frac{1}{2304} \left(\frac{\check{S}}{\sim}\right)^3 r^6 \right] \exp(-\check{S}t) \tag{30}$$

If the velocity is divided by its maximal value  $u_{\max}(t) = \exp(-\check{S}t)$ , then the time-independent solution is obtained, which is easy for comparison:

$$\frac{u_z}{u_{\max}} = 1 - \frac{1}{4} \frac{\check{S}}{\sim} r^2 + \frac{1}{64} \left(\frac{\check{S}}{\sim}\right)^2 r^4 - \frac{1}{2304} \left(\frac{\check{S}}{\sim}\right)^3 r^6 \tag{31}$$

This is the formula that will be used for code validation.

The analyzed case for three dimensional example is an infinite long pipe with radius  $R = 1$ . This case is simplified by assuming periodicity in the  $z$ -direction (longitudinal), thus reducing the computational length of the pipe to a few points. The axis of symmetry of the pipe is also used, which allowed for further reduction of the entire circular cross section of the pipe to just a fraction of a circle with a small angle (few points) and a radius of one. For such a simplified case, a mesh representing a slice of the pipe is generated, as shown in Figure 10. The boundary conditions are set as follows: in the  $z$ -and  $\sim$ -directions, the

periodic boundary condition is applied; in the  $r$ -direction, a symmetry boundary condition is applied at the center ( $r = 0$ ) and at the pipe wall ( $r = 1$ ), a non-slip boundary is applied. The symmetry boundary condition is zero for all velocities in the normal direction to the boundary:

$$\frac{\partial u_i}{\partial n} = 0 \quad (31)$$

The initial conditions are  $u_z = 1$ , and the others are zero.

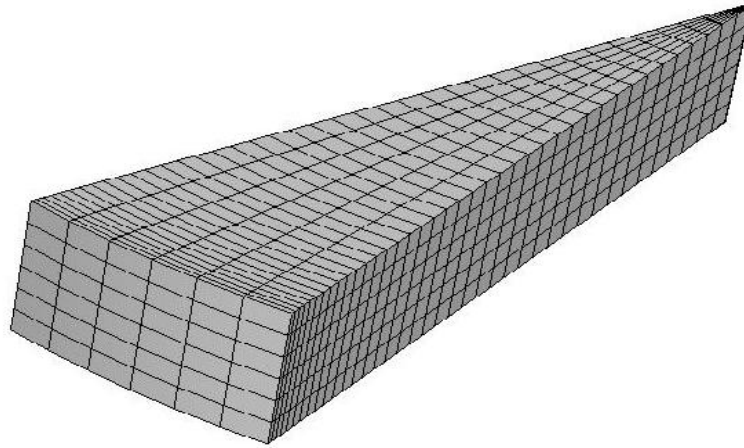


Figure 10. Finite element mesh.

Figure 11 illustrates the development of flow with time in the infinite long pipe. It can be clearly seen that at the start of the solution the velocity profile was flat. However, with the passage of time the velocity profile became nearly parabolic, and the values of the velocity in the  $z$ -direction (blue) in the middle of the slice along the radius compared very well with the analytically calculated values (green), as shown in the plot. Figures 12 and 13 show the velocity contour plot and vector plot of the velocity, respectively, in the  $z$ -direction. It is evident that velocity is zero at the outer end of the pipe, due to the wall, and maximum at the centre of the pipe as flow is passing through it.

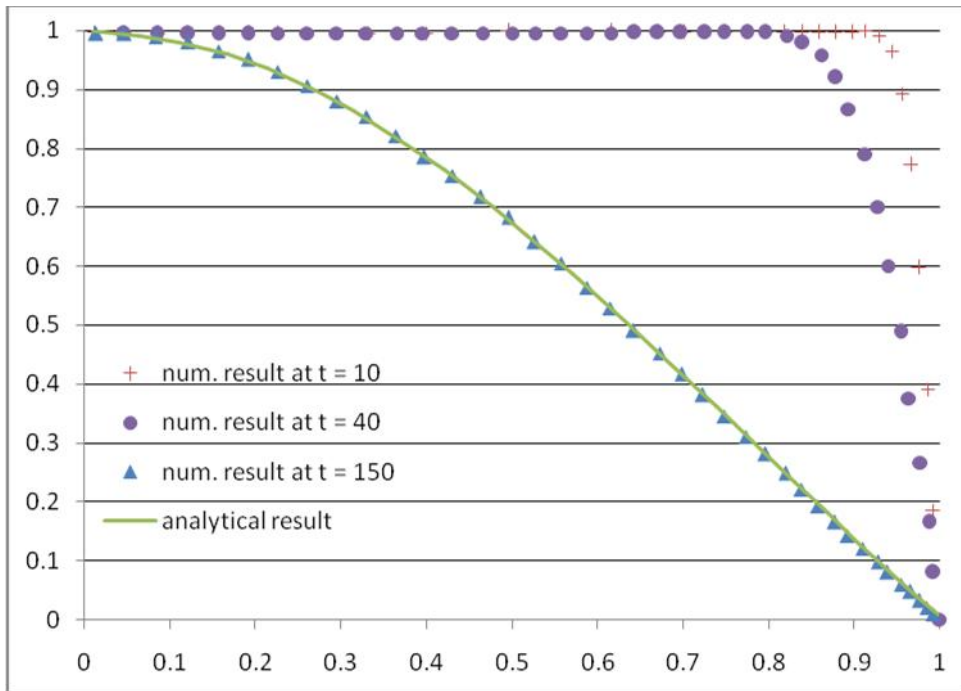


Figure 11. Velocity profile and comparison with analytical result.

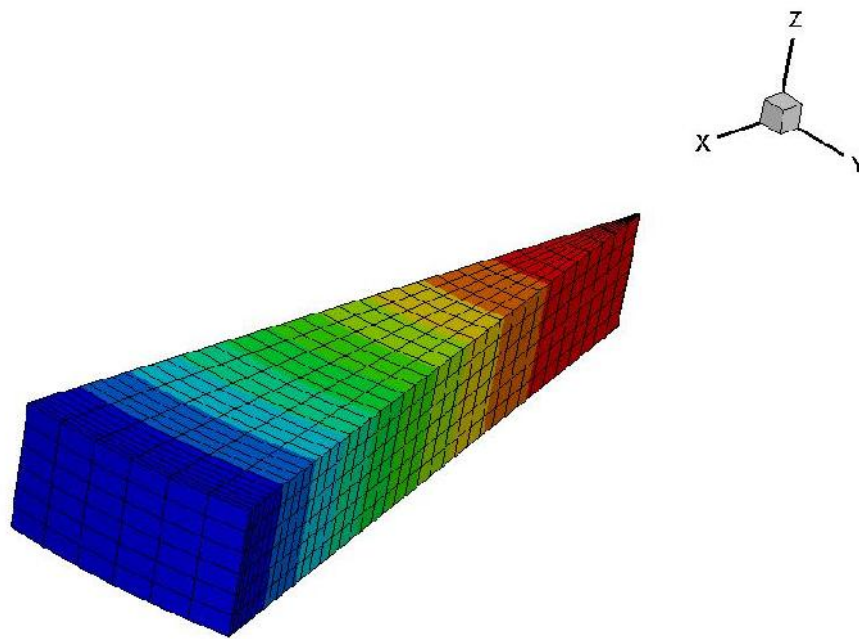


Figure 12. Velocity contour for flow in pipe.

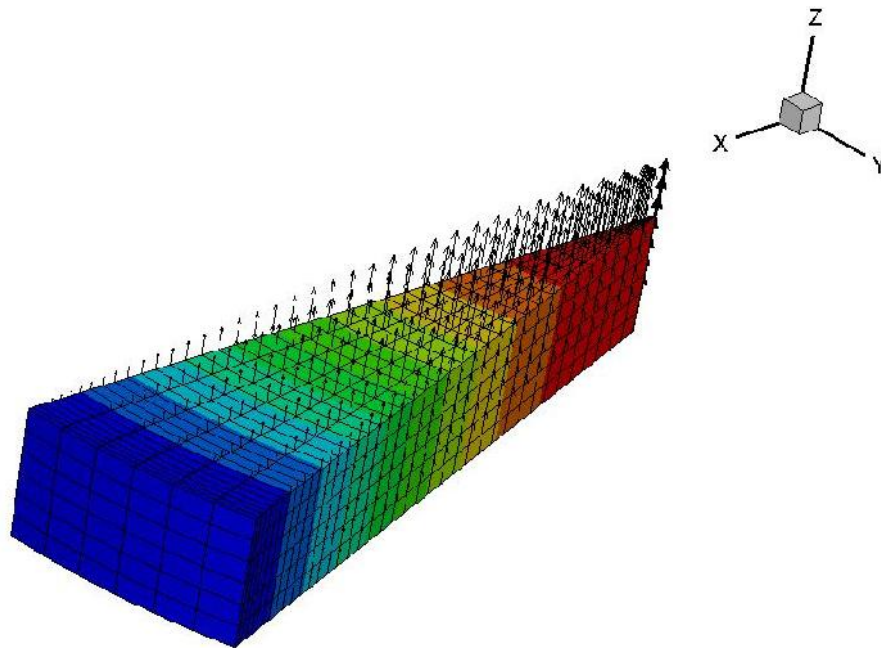


Figure 13. Vector plot for flow in pipe.

#### 4. Conclusion

A WENO/compact scheme for solving the two-dimensional incompressible Navier-Stokes equations has been presented. The convective part of the N-S equations is solved using fifth order WENO spatial operators, and the diffusion terms are solved with a sixth-order compact central difference scheme. The third-order TVD Runge-Kutta explicit time-integrating scheme is adopted for the unsteady flow computations. Test cases, driven cavity flow, Taylor Green vortex test, double shear layer, and backward-facing step are performed to investigate the accuracy and efficiency of the scheme. Skewed driven cavity has been analyzed in order to study the functioning of proposed scheme in generalized coordinates. Infinite long pipe is tested for codes functionality in three dimensions. Results are compared with available established data in the literature and are in good agreement with the published data. It has been shown that due to the control adaptive dissipation property of WENO, the solver can capture the general flow features with coarser grid size. The code is thus grid efficient and fifth order accuracy is obtained for velocity variables. Another advantage of using this shock capturing scheme is that the developed three dimensions code can be used for the direct numerical simulation of the turbulence problems in future. Achieving the results by using fewer nodes will be very helpful in such kind of analysis in terms of computational efficiency.

#### References

- [1] Chorin, A.J., *Numerical solution of the Navier-Stokes equations*. Mathematics of Computation, 1968. 22: pp.745-762.
- [2] Drikakis, D. and Rider, W., *High-resolution methods for incompressible and low-speed flows*. Springer-Verlag, Berlin, 2005.
- [3] Kim, J. and Moin, P., *Application of a fractional-step method to incompressible Navier-Stokes equations*. Journal of Computational Physics, 1984. 59: pp. 308-323.
- [4] Moin, P. and Kim, J., *On the numerical solution of time dependent viscous incompressible fluids flow involving solid boundaries*. Journal of Computational Physics, 1980. 35: pp. 381.
- [5] Orszag, S.A. and Israeli, M., *Numerical simulation of viscous incompressible flow*. Annual Review of Fluid Mechanics, 1974. 6: pp. 281-318.

- [6] Harlow, F.H. and Welsh, J.E., *Numerical calculation of time dependent viscous incompressible fluid with free surface*. Phys. Fluids, 1965. 8: pp. 2182.
- [7] Rogers, S.E., *Numerical solution of incompressible Navier-Stokes equations*. NASA TM 102199, Ames Research Center, Moffett Field, CA, 1990.
- [8] Shu, C.W. and Osher, S., *Efficient implementation of essentially non-oscillatory shock capturing schemes II*. Journal of Computational Physics, 1989. 83: pp. 32-78.
- [9] Shu, C.W., Zang, T.A., Erlebacher, G., Whitaker, D., and Osher, S., *High order ENO schemes applied to two- and three- dimensional compressible flow*. Applied Numerical Mathematics, 1992. 9: pp. 45-71.
- [10] Bell, J., Colella, P. and Glaz, H., *A second order projection method for the incompressible Navier- Stokes equations*. Journal of Computational Physics, 1989. 85: pp. 257-283.
- [11] Harten, A., Engquist, B., Osher, S., and Chakravarthy, S., *Uniformly high order essentially non-oscillatory schemes, III*. Journal of Computational Physics, 1987. 71: pp. 231-303.
- [12] Shu, C.W. and Osher, S., *Efficient implementation of essentially non-oscillatory shock capturing schemes*. Journal of Computational Physics, 1988. 77: pp. 439-471.
- [13] Liu, X.D., Osher, S. and Chan, T., *Weighted essentially non-oscillatory schemes*. Journal of Computational Physics, 1994. 115: pp. 200-212.
- [14] Jiang, G. and Shu, C.W., *Efficient implementation of weighted ENO schemes*. Journal of Computational Physics, 1996. 126: pp. 202-228.
- [15] Adams, N. and Shariff, K., *A high-resolution hybrid compact-ENO scheme for shock-turbulence interaction problems*. Journal of Computational Physics, 1996. 127: pp. 27-51.
- [16] Walsteijn, F., *Robust numerical methods for 2D turbulence*. Journal of Computational Physics, 1994. 114: pp. 129-145.
- [17] Ladeinde, F., O'Brien, E., Cai, X., and Liu, W., *Advection by polytropic compressible turbulence*. Physics of Fluids, 1995. 7: pp. 2848-2857.
- [18] Jiang, G.S. and Shu, C.W., *Efficient implementation of weighted ENO schemes*. Journal of Computational Physics, 1996. 126: pp. 202-228.
- [19] Arshed, G.M. and Hoffmann, K.A., *Implementation of improved WENO scheme to higher dimensions in relation to shock-turbulence interaction*. Proceedings of 47<sup>th</sup> AIAA Aerospace Sciences Meeting, AIAA-2009-1313, Orlando, Florida, January 2009.
- [20] Chen, Y.N., Yang, S.C., and Yang, J.Y., *Implicit weighted essentially non-oscillatory schemes for the incompressible Navier-Stokes equation*. International Journal for Numerical Methods in Fluids, 1999. 31: pp. 747-765.
- [21] Hsieh, T.J., Wang, C.H., and Yang, J.W., *Numerical experiments with several variant WENO schemes for Euler equations*. International Journal for Numerical Methods in Fluids, 2008. 58: pp. 1017-1039.
- [22] Shu, C.W., *Essentially non-oscillatory and weighted essentially non-oscillatory schemes for hyperbolic conservation laws*. NASA/CR-97-206253, Institute for Computer Applications in Science and Engineering, NASA Langley Research Center, Hampton, VA, 1997.
- [23] Khurshid, H., and Hoffmann, K.A., *Implementation of WENO scheme to the incompressible Navier-Stokes equations in generalized coordinate system*. 40<sup>th</sup> Fluid Dynamics conference and Exhibit, AIAA, July 2010, Chicago, USA
- [24] Botella, O., and Peyret, R., *Benchmark spectral results on the lid-driven cavity flow*. Comput. Fluids, 1998. 27: pp. 421-433
- [25] Schreiber, R., and Keller, H.B., *Driven cavity flow by efficient numerical techniques*. Journal of Computational Physics, 1983. 49: pp. 310-333
- [26] Erturk, E., and Gokcol, C., *Fourth order compact formulation of Navier-Stokes equations and driven cavity flow at high Reynolds Numbers*. International Journal of Numerical Methods in Fluids, 2006. 50: pp. 421-436

- [27] Wright, N.G, and Gaskell, P.H., *An efficient multigrid approach to solving highly recirculating flows techniques,*” Computer and Fluids, 1995. 24:, pp. 63-79
- [28] Benjamin, A.S., and Denny, V.E., *On the convergence of numerical solutions for 2-D flows in a cavity at large Re.* Journal of Computational Physics, 1979. 33: pp. 340-358
- [29] Nishida, H., and Satofuka, N., *Higher order solutions of square driven cavity flow using a variable order multi grid method.* International Journal of Numerical Methods in Fluids, 1992. 34: pp. 637-653
- [30] Erturk, E., Corke, T.C., and Gokcol, C., *Numerical solutions of 2-D steady incompressible driven cavity flow at high Reynolds numbers.* International Journal of Numerical Methods in Fluids, 2005. 48: pp. 747-774
- [31] Li, M., Tang, T., and Fornberg, B., *A compact fourth order finite difference scheme for the steady incompressible Navier-Stokes equations.* International Journal of Numerical Methods in Fluids, 1995. 20: pp. 1137-1151
- [32] Armaly, B.F., Durst, F., Pereira, J.C.F, and Schonung, B., *Experimental and theoretical investigation of backward facing step flow.* Journal of fluid Mechanics, 1983. 127: pp. 473-496.
- [33] Choi, H.W and Barakat, A.I., *Numerical study of the impact of non Newtonian blood behavior on flow over a two dimensional backward facing step.* Biorheology, 2005. 42: pp. 493-509.
- [34] Demirdzic, I., Lilek, Z., and Peric, M., *Fluid flow and heat transfer test problems for non-orthogonal grids: Bench mark solutions.* International Journal for Numerical Methods in Fluids, 1992. 15: pp. 329-354.
- [35] Erturk, E., and Dursun, B., *Numerical solutions of 2-D steady incompressible flow in a driven skewed cavity.* Journal of Applied mathematics and Mechanics, 2007. 87: pp. 377-392
- [36] Oosterlee, C.W., Wessling, P., Segal, A., and Brakkee, E., *Benchmark solutions for the incompressible Navier-Stokes equations in general co-ordinates on staggered grids.* International Journal of Numerical Methods in Fluids, 1993. 17: pp. 301-321
- [37] Shklyar, A., and Arbel, A., *Numerical method for the calculation of incompressible flow in general curvilinear co-ordinates with double staggered grid.* International Journal of Numerical Methods in Fluids, 2003. 45: pp. 741-763